Published in final edited form as:
Sci Transl Med. 2012 August 15; 4(147): 147ra112. doi:10.1126/scitranslmed.3003778.

Targeted tumor-penetrating siRNA nanocomplexes for credentialing the ovarian cancer target *ID4*

Yin Ren[1,*], **Hiu Wing Cheung**[2,3,*], **Geoffrey von Maltzhan**[1], **Amit Agrawal**[1], **Glenn S. Cowley**[3], **Barbara A. Weir**[3], **Jesse S. Boehm**[3], **Pablo Tamayo**[3], **Alison M. Karst**[2], **Joyce F. Liu**[2], **Michelle S. Hirsch**[7], **Jill P. Mesirov**[3,9], **Ronny Drapkin**[2,7], **David E. Root**[3], **Justin Lo**[1], **Valentina Fogal**[4,5], **Erkki Ruoslahti**[4,5], **William C. Hahn**[2,3,6,8,†], and **Sangeeta N. Bhatia**[1,3,6,9,10,†]

[1] Health Sciences and Technology, Massachusetts Institute of Technology, Cambridge, MA 02139

[2]Department of Medical Oncology, Dana-Farber Cancer Institute, Boston, MA 02115

[3]Broad Institute of Harvard and MIT, Cambridge, MA 02142

[4]Center for Nanomedicine, Sanford-Burnham Medical Research Institute, University of California, Santa Barbara, CA 93106-9610

[5]Cancer Center, Sanford-Burnham Medical Research Institute, La Jolla, CA 92037

[6]Department of Medicine, Brigham and Women's Hospital and Harvard Medical School, Boston, MA 02115, USA

[7]Department of Pathology, Brigham and Women's Hospital and Harvard Medical School, Boston, MA 02115, USA

[8]Center for Cancer Genome Discovery, Dana-Farber Cancer Institute, Boston, MA 02115

[9]Electrical Engineering and Computer Science and David H. Koch Institute for Integrative Cancer Research, Massachusetts Institute of Technology, Cambridge, MA 02139

[10]Howard Hughes Medical Institute, Chevy Chase, Maryland 20815, USA.

Abstract

The comprehensive characterization of a large number of cancer genomes will eventually lead to a compendium of genetic alterations in specific cancers. Unfortunately, the number and complexity of identified alterations complicate endeavors to identify biologically relevant mutations critical for tumor maintenance, because many of these targets are not amenable to manipulation by small molecules or antibodies. RNAi provides a direct way to study putative cancer targets; however,

[†]To whom correspondence should be addressed. william_hahn@dfci.harvard.edu (W.H.C.); sbhatia@mit.edu (S.N.B.)..
[*]These authors contributed equally.

Author contributions: Y.R., H.W.C., G.S.C., B.A.W., J.S.B., D.E.R., W.C.H., and S.N.B. designed the experiments. Y.R., G.V.M., A.A., and S.N.B. designed the peptide screen. Y.R. characterized TPN. G.S.C., J.S.B., B.A.W., D.E.R., and W.C.H. supervised RNAi screens. B.A.W., J.S.B., H.W.C., G.S.C., R.D., P.T., J.P.M., D.E.R., and W.C.H. analyzed the RNAi data. H.W.C., and A.M.K. performed experiments with transformation and shRNAs. B.A.W., H.W.C., and J.S.B. performed expression profiling and analysis. Y.R., H.W.C., W.C.H., and S.N.B. analyzed the integrated RNAi data. J.L. assisted with biodistribution studies. M.S.H. and J.F.L. analyzed the tissue-microarray. V.F. and E.R. provided advice, reagents and analysis on tumor targeting aspects of the work. Y.R., H.W.C., W.C.H., and S.N.B. wrote the manuscript. All authors discussed the results and commented on the manuscript.

Competing interests: E.R. is a shareholder of CendR Inc, which licenses the iRGD peptide. A patent has been filed by M.I.T. describing the tumor-penetrating nanocomplexes.

Data and materials availability: All data files can be assessed at the Integrative Genomics portal (http://www.broadinstitute.org/IGP/home). An MTA is required for distribution of the primary FT epithelial cells (A.M.K).

specific delivery of therapeutics to the tumor parenchyma remains an intractable problem. We describe a platform for the discovery and initial validation of cancer targets, composed of a systematic effort to identify amplified and essential genes in human cancer cell lines and tumors partnered with a novel modular delivery technology. We developed a tumor-penetrating nanocomplex (TPN) comprised of siRNA complexed with a tandem tumor-penetrating and membrane-translocating peptide, which enabled the specific delivery of siRNA deep into the tumor parenchyma. We employed TPN *in vivo* to evaluate *inhibitor of DNA binding 4* (*ID4)* as a novel oncogene. Treatment of ovarian tumor-bearing mice with *ID4*-specific TPN suppressed growth of established tumors and significantly improved survival. These observations not only credential *ID4* as an oncogene in 32% of high-grade ovarian cancers, but also provide a framework for the identification, validation, and understanding of potential therapeutic cancer targets.

INTRODUCTION

Genome-scale studies of cancer samples have begun to provide a global depiction of genetic alterations in human cancers, but the complexity and volume of data that emerge from these efforts has made dissecting the underlying biology of cancer difficult, and little is known about the functions of most of the candidates that emerge. For example, in studies of 489 primary high-grade serous ovarian cancer genomes, 1825 genes were identified as targeted by recurrent amplification events (1). Systematic approaches to study the function of genes in cancer cell lines, such as genome-scale, pooled short hairpin RNA (shRNA) screens, offer a means to assess the consequences of the genetic alterations found in s uch genome characterization efforts. We recently used a shRNA-based approach to find genes that are both overexpressed in human primary tumors and also essential for the proliferation of ovarian cancer cells (2). This approach identified 54 overexpressed and essential genes in ovarian cancer and 16 genes in non-small cell lung cancer (NSCLC) that required further validation *in vivo*. Furthermore, many of these candidates represent targets that are not amenable to antibody-based therapeutics or traditional small molecule approaches. Thus, if one envisions a discovery pipeline that begins with cancer genomes and ends with novel therapeutics, there is clearly a bottleneck at the point of *in vivo* validation of novel targets.

Achieving silencing in the epithelial cells in the tumor parenchyma is especially critical to study the genetic alterations of interest. RNA interference (RNAi) is a potentially attractive means to silence expression of candidate genes *in vivo*, particularly for “undruggable” gene products (3-4). However, systemic delivery of small interfering RNA (siRNA) to tumors has been challenging owing to rapid clearance, susceptibility to serum nucleases, and endosomal entrapment of small RNAs, in addition to their inherent inadequate tumor penetration (5). Tumor penetration is also a problem for the delivery of siRNA and shRNA, among other cargo, and is characterized by limited transport into the extravascular tumor tissue beyond the perivascular region (6). This low penetration is thought to arise from the combination of dysfunctional blood vessels that are poorly perfused, and a high interstitial pressure, especially in solid tumors, in part due to dysfunctional lymphatics (7). The leakiness of tumor vessels partially counteracts the poor penetration (the so-called enhanced permeability and retention, or EPR, effect), but the size-dependence and variability of this property can limit its usefulness (7). Desmoplastic stromal barriers can further impede transport of therapeutics through tumors (8-9).

A new class of tumor-penetrating peptides has been described recently, which home to several types of tumors and leverage a consensus R/KXXR/K C-terminal peptide motif [the C-end rule (CendR)] to stimulate transvascular transport and rapidly deliver therapeutic cargo deep into the tumor parenchyma (10-11). These peptides are tumor-specific, unlike

canonical cell-penetrating peptides that do not display cell or tissue-type specificity (12), and are able to improve the delivery of small molecules, antibodies, and nanoparticles (13). Despite their promise, this class of peptides has not been successfully co-opted for siRNA delivery, in part owing to the additional challenges of delivering oligonucleotides across cell membranes, out of endosomes, and into the cytosol to achieve gene silencing.

Here, we designed a siRNA delivery vehicle that was tumor-penetrating and modular, so it could be easily assembled in a single step to accommodate different payloads to various genes of interest. We envision that such a technology would enable a platform wherein novel targets can be identified using structural and functional genomics and subsequently rapidly "credentialed" both *in vitro* and *in vivo*. Follow-up studies could then identify the mechanism of action underlying the observations and establish (and ultimately prioritize) novel oncogenes as therapeutic targets. To achieve this goal, we have combined a systematic effort to identify genes that are both essential and genetically altered in human cancer cell lines and tumors with the development and deployment of a novel tumor-specific and tissue-penetrating siRNA delivery platform.

RESULTS

Identification of *ID4* as an essential oncogene in human ovarian cancer

To facilitate the identification of genes that are essential in specific cancer types, we initiated Project Achilles, a large-scale effort involving genome-scale, pooled shRNA screens in human cancer cell lines (2). Recent efforts to characterize the genomes of primary high-grade serous ovarian cancer have revealed 63 recurrent regions of copy number gain and 50 regions of copy number loss, each containing several genes (1). To identify genes that are both recurrently amplified and essential in ovarian cancers that harbor increased copy number of these genes, we quantified the distribution of shRNA proliferation scores among all shRNAs for each amplified gene (Fig. 1A). We identified 206 cases in which shRNAs targeting the amplified gene were significantly depleted ($P<0.05$, z-score), including known ovarian cancer oncogenes *KRAS, AKT1, BCL2L1*, and *ERBB3*, and newer candidates for ovarian cancer, including the *inhibitor of DNA binding 4* (*ID4)* transcriptional regulatory protein and the *S-phase kinase-associated protein 2* (*SKP2*) E3-ubiquitin ligase (table S1).

We selected *ID4*, a helix-loop-helix (HLH) transcriptional regulator, for further study because recent genomic analyses have indicated that the chromosomal region containing *ID4* (6p22) is amplified in 32% of high-grade serous ovarian cancers (1) (Fig. 1B). Also, *ID4* is overexpressed in the majority of primary ovarian cancers, but not in normal ovary, fallopian tube, and other tissues (Fig. 1C; fig. S1A). In addition, by examining the transcript levels of *ID4* in a large panel of cancer cell lines, we found that *ID4* was frequently overexpressed in the majority of ovarian cancer cell lines and cell lines derived from other cancer lineages, such as endometrial cancer, breast cancer, and glioblastoma (fig. S1B).

After identifying *ID4* as a candidate oncogene in human samples, our next step was to establish preclinical models to credential the oncogenic potential of *ID4*, specifically by investigating the relationship between amplification, expression, and essentiality of *ID4* in a panel of human cancer cell lines. First, we found that multiple shRNAs that did not alter the expression of *ID1, ID2*, and *ID3*, but suppressed *ID4* (fig. S1C), significantly inhibited the proliferation of 9 out of 11 ovarian cancer cell lines and two glioblastoma cell lines tested (range 53-92%) (Fig. 1D). Ovarian cancer cell lines OVCAR-8, OVCAR-4, and CaOV-3, which harbor increased copy number (Fig. 1E) and exhibit overexpression of *ID4* (Fig. 1D), died by apoptosis after *ID4* suppression (fig. S1D). By contrast, 7 cell lines that express

comparatively lower *ID4* levels showed little inhibition of proliferation after *ID4* suppression (range 0-44%) (Fig. 1D).

We then tested whether *ID4* was an oncogene by investigating its ability to induce cell transformation. Expression of oncogenic $HRAS^{V12}$ or co-expression of known RAS effectorsrenders immortalized human epithelial cells tumorigenic *in vivo* (14). Therefore, to investigate the role of *ID4* in human ovarian epithelial cells, we similarly created an ovarian surface epithelial cell line expressing the SV40 Large T and small t antigens, hTERT, and MEK^{DD} (IOSE-M cells) (fig. S1E), and used this cell line to identify genes that promote tumorigenicity. Expression of *ID4* at levels found in ovarian cancer cell lines did not affect the cell cycle progression (fig. S1F) but dramatically increased the rate of tumor formation *in vivo* compared to cells expressing a control vector (Fig. 1F). Addition of *ID4* that harbored mutations in the HLH domain, or the addition of *ID1, ID2*, or *ID3*, each failed to confer significant tumorigenicity (Fig. 1F).

Recent work suggests that the majority of ovarian cancers arise from the fallopian tube (FT) epithelium rather than the ovarian surface epithelium (15). As such, we used immortalized FT epithelial cells (16) and assessed whether *ID4* expression also induced cell transformation in these cells. As we found for ovarian epithelial cells, *ID4* induced anchorage-independent growth in FT cells (Fig. 1G). These observations show that *ID4* is amplified, essential, and transforming in ovarian epithelial cells.

ID4 induces transformation by regulating the *HOXA9* and *CDKN1A* transcriptional programs

To explore the mechanism of action by which *ID4* induces transformation, we performed gene expression profiling in immortalized ovarian surface epithelial (IOSE-M) cells that overexpress *ID4* or a control vector. Among the top 5 gene sets, we found highly significant enrichment of 3 gene sets upregulated by expression of the oncogenic Nucleoporin 98-Homeobox A9 (NUP98-HOXA9) fusion protein (17) (Fig. 2A; fig. S2). These 3 gene sets represent short-term (6 h) and long-term (3 and 8 days) upregulation after induction of *NUP98-HOXA9*. *ID4* expression in IOSE-M cells consistently increased expression of multiple *HOXA* genes, including *HOXA9, HOXA7*, and *HOXA3* (Fig. 2B); whereas suppression of *ID4* led to significantly reduced levels of these same genes (Fig. 2C; fig. S3A). To determine whether *HOXA9* was required for *ID4*-induced cell transformation, we introduced three previously validated *HOXA9*-specific shRNAs (18) or control shRNAs targeting green fluorescent protein (sh*GFP*) into *ID4*-overexpressing IOSE-M cells (fig. S3B). Suppression of *HOXA9* only slightly (~30%) reduced cell proliferation (fig. S3C), but significantly inhibited *ID4*-induced anchorage-independent growth (Fig. 2D) and reduced the rate of tumor formation *in vivo* compared to control sh*GFP* (Fig. 2E).

Finally, to confirm these observations in human ovarian cancers, we analysed the expression profiles from primary ovarian tumors by TCGA project (1) and found that many genes within the *NUP98-HOXA9* expression signature (TAKEDA_TARGETS OF NUP98-HOXA9 FUSION_10D_DN) were significantly downregulated in tumors that express low levels of *ID4* (Fig. 2F). The gene set was originally defined 10 days after expression of *NUP98-HOXA9.* Human tumors that harbored *ID4* amplifications showed significantly increased expression of a gene set that was downregulated by $p21^{WAF1/CIP1}$ or *TP53* tumor suppressor (P21_P53_ANY_DN) (19), indicating a suppressed $p21^{WAF1/CIP1}$ transcriptional activity in *ID4*-amplified tumors (Fig. 2G). These observations demonstrate that expression or amplification of *ID4* regulates the *HOXA9* and *CDKN1A* transcriptional programs to disrupt the normal regulation of proliferation and differentiation.

Design of tumor-penetrating nanocomplexes (TPN)

To assess whether *ID4* functions as a therapeutic target for ovarian cancer, we designed a siRNA delivery platform that permits access to specific cancer cells. To this end, we synthesized a library of tandem peptides capable of tumor-homing and penetration (with a fixed cyclic domain) and siRNA delivery across cell membranes (variable linear domains for electrostatic binding) (Fig. 3A; table S2). We selected the cyclic nonapeptide LyP-1 (CGNKRTRGC) as the tumor-penetrating domain for all tandem peptides because it binds p32 (p33/gC1q receptor/HABP1), a mitochondrial protein whose expression is elevated on the surface of stressed tumor and tumor-associated cells in a wide range of tumor types (20). Once bound, LyP-1 is proteolytically processed by endogenous proteases to reveal a cryptic CendR motif that activates tissue penetration of associated payloads and results in higher therapeutic accumulation (11, 21).

We postulated that a tandem peptide consisting of an N-terminal cell-penetrating peptide (CPP) with a C-terminal LyP-1 separated by a 4-glycine linker domain would retain membrane translocation and tissue-penetrating properties, condense siRNA into nanoparticles, and selectively target tumor cells expressing p32 at the surface. We created a library of 18 linear membrane-translocation domains that contained both polycationic peptide sequences [oligoarginines of varying net charge, TAT (48-60), and the HSV-1 tegument protein VP22] and amphipathic sequences [Penetratin (PEN) and Transportan (TP)]. Inspired by nonenveloped RNA viruses (22), a myristoyl group was added to the amino terminus to facilitate interactions with membrane lipids (Fig. 3B; fig. S4A). We first confirmed that peptides from the library bound siRNA electrostatically to form stable nanocomplexes in water (diameter ~80 nm), phosphate-buffered saline (PBS, diameter ~200-400 nm), and serum (diameter ~200-400 nm) (fig. S4, B and C). The majority of peptides were noncytotoxic, with the exception of highly cationic peptides 12R and 15R (fig. S4D).

To evaluate nanocomplex-mediated gene silencing, we treated HeLa cells expressing destabilized GFP with si*GFP* bound to either tandem peptides or lipofectamine. The top three carriers—6R, 9R, and TP—silenced GFP expression 40-60% (Fig. 3C). Flow cytometry analysis indicated that gene suppression was dose-dependent and heterogeneous across the cell population, with 50-70% of cells exhibiting near-complete gene suppression (fig. S4E), with variation likely owing to heterogeneity in p32 expression. *GFP* suppression can underreport the magnitude of silencing endogenous gene targets, such as amplified oncogenes (23); thus, we used this assay to compare peptides, but not as a quantitative measure of efficiency of RNAi of oncogenes. We chose nanocomplexes consisting of siRNA bound to TP-LyP-1 for further analysis (hereby referred to as the tumor-penetrating nanocomplex, or TPN), as it had the highest efficacy in delivering siRNA to cells, was potent relative to other tandem peptides (>25% gene suppression at 25 nM siRNA), and has a known secondary structure (24), in contrast to poly-Arg peptides.

Next, we examined the specificity of receptor targeting and gene suppression. Uptake of LyP-1–targeted nanocomplexes was significantly higher than control nanocomplexes bearing ARAL (ARALPSQRSR), a peptide that has the same net charge as LyP-1 (fig. S4F). LyP-1 targeting was specific, as shown by competition assays with free LyP-1 (fig. S4G) and in cells lacking the p32 receptor (fig. S4H). We did not detect statistically significant alterations in GFP expression in HeLa cells exposed to untargeted control nanocomplexes (UCN) carrying si*GFP* (TP-ARAL/si*GFP*) or targeted TP-LyP-1 carrying a scrambled siRNA sequence (TP-LyP-1/si*UT*) (Fig. 3D). In contrast, when we used TP-LyP-1 carrying si*GFP*, we observed over 40% suppression of GFP expression.

OVCAR-4 and OVCAR-8 human ovarian cancer cell lines have elevated surface p32 expression (fig. S5); therefore, these cell lines were compatible for testing TPN-mediated delivery of *ID4*-specific siRNA (si*ID4*). When *ID4* was suppressed in these cell lines *in vitro* using TPN (Fig. 4A), we observed a decrease in cell viability (Fig. 4B) and an increased rate of apoptosis (fig. S5; Fig. 4C). We therefore selected the OVCAR-4 and OVCAR-8 ovarian cancer cell lines for our preclinical evaluation of *ID4 in vivo*.

TPN homing and penetration *in vivo* in mice

For *in vivo* applications, an ideal carrier should extend the half-life of siRNA in serum by protecting it from nuclease degradation, yet readily dissociate from siRNA once in the cytosol of target cells. We used a gel-shift assay to determine an optimal siRNA-to-peptide complexation molar ratio of 1:20, at which free siRNAs were encapsulated into TPN, likely owing to charge-based interactions between the peptide and the siRNA backbone (Fig. 5A). We found that TPN extended the stability of siRNA to >12 h in murine serum (Fig. 5A), and the size of TPN remained stable in the presence of serum over the course of 10 hours (Fig. 5B). Furthermore, we observed unpackaging of TPN upon exposure to endolysosomal pH (5.3-6.5) (Fig. 4D).

We assessed whether TPN enabled receptor-specific, tumor-penetrating siRNA delivery to established tumors (Fig. 5C), by examining their *in vivo* homing behavior in mice bearing subcutaneous human melanoma tumors (MDA-MB-435 xenografts). After intravenous administration, most siRNAs were cleared renally, as indicated by bladder accumulation of siRNA over 8 hours (fig. S6A). However, we also observed that TPN was cleared more slowly than naked siRNA (Fig. 5D) and distributed to tumor tissues within 30 minutes (fig. S6B). We noted similar pharmacokinetics for intravenous and intraperitoneal injection of TPN, suggesting the potential for multiple routes of administration (Fig. 5D; fig. S6A).

Biodistribution studies showed blood clearance through liver and spleen accumulation likely owing to reticuloendothelial uptake. TPN also distributed to the lung (fig. S6C and D), a common uptake site for passively targeted nanoparticles owing to interactions with the first capillary bed following intravenous injection (25). After clearance from circulation (4 h), we found an over three-fold increase in the tumor fluorescence of TPN in MDA-MB-435 xenografts compared to UCN (Fig. 5E). Similar results in tumor-targeting were obtained in mice bearing OVCAR-8 ovarian tumor xenografts (fig. S6E).

Although bulk tumor accumulation provides a global measure of targeting, it does not provide spatial information on the extravascular and tumor interstitial availability of TPN, which ultimately determines their efficacy. We thus performed histological characterization of TPN penetration in xenografted subcutaneous OVCAR-8 tumors at various time points and found that these TPN exhibited an initial intravascular distribution and subsequently extravasated into the tumor interstitium (Fig. 5F). The fraction of TPN that were sequestered beyond the intravascular space was significantly higher than that of UCN (Fig. 5F). Furthermore, TPN accumulated in the tumor parenchyma to a similar degree as nanocomplexes bearing a different tumor-penetrating motif, iRGD (CRGDKGPDC) (10). Non-penetrating, targeted nanocomplexes (TP-RGD4C) (26) or the commercial reagent lipofectamine failed to show a similar distribution (Fig. 5G). We also found TPN also co-localized with p32-positive tumor cells, as expected, but failed to detect UCN or naked siRNAs in tumors (fig. S6F). This pattern of distribution is similar to previously reported LyP-1 peptide (21) and LyP-1 targeted nanoparticle homing (27).

Loss of tumor maintenance after TPN-mediated suppression of *ID4 in vivo*

We next tested whether *ID4* was essential for tumor maintenance through TPN-mediated delivery of si*ID4* in established human ovarian cancer xenografts *in vivo*. Mice harboring subcutaneous OVCAR-4 tumors were injected intravenously or intraperitoneally with TPN/si*ID4* every 3 days for 25 days. Control animals with tumors were injected intravenously with saline, TP-LyP-1 carrier without siRNA, or TPN/si*GFP*. Repeated, systemic administration of the TPN/si*ID4* resulted in 80-90% decrease in *ID4* mRNA relative to treatment with TPN/si*GFP* (Fig. 6A), with a corresponding suppression of tumor growth by 82% in IV-injected and 87% in IP-injected animals (Fig. 6B, D). Tumor growth was static in si*ID4*-treated cohorts for 30 days after the termination of TPN treatment (Fig. 6B). In contrast, TPN/si*GFP* or TP-LyP-1 carrier had no effect on *ID4* and did not prevent further tumor growth. We also found that both methods of TPN/si*ID4* injection induced a significant increase in *cyclin-dependent kinase inhibitor 1A* (*CDKN1A*, $p21^{WAF1/CIP1}$) transcript levels (Fig. 6C), a known target of *ID4* in mediating cell-cycle arrest (28). Residual TPN/si*ID4*-treated tumors exhibited significant apoptosis (Fig. 6E).

We then tested whether TPN/si*ID4* could induce therapeutic activity in mice harboring disseminated tumors. We established orthotopic OVCAR-8 tumors, confirmed intra-abdominal dissemination three weeks after implantation, and then initiated intraperitoneal injection of TPN every 3 days for 30 days. The tumor burden in mice that received TPN/si*ID4* remained low compared to controls (Fig. 7A; fig. S7A), and 80% of the recipients of TPN/si*ID4* (IP) survived more than 60 days, even after the nanocomplex treatments ceased at day 50 (Fig. 7B). After 40 days, disseminated tumors and hemorrhagic ascites were present in control cohorts (fig. S7B), but there was no visible tumor lesions in 4 out of 5 TPN/si*ID4*–treated mice upon necropsy, indicating tumor regression. Histological analysis of the single visible remnant tumor in a si*ID4*-treated animal revealed significant reduction in *ID4* levels relative to tumors from the three control cohorts and increased apoptosis in the tumor parenchyma (Fig. 7C; fig. S7C).

The versatility of TPN for direct target comparison was demonstrated by treating mice bearing OVCAR-8 tumors with TPN carrying siRNA against *Claudin-3* (*CLDN3*), a recently reported potential ovarian siRNA target (29). TPN/si*CLDN3* led to initial reduction of tumor growth compared to controls treated with saline or TP-LyP-1 carrier alone, but was unable to achieve sustained growth suppression compared to TPN/si*ID4* treatments. (fig. S7D).

Side effects of TPN administration *in vivo*

In some cases, apparent therapeutic effects of RNAi may be confounded by non-sequence-specific innate immune responses (30). Therefore, we independently measured serum levels of interferon α (IFN-α), tumor necrosis factor α (TNF-α), and interleukin 6 (IL-6) in immunocompetent mice after administering various TPN-based siRNA formulations, and failed to observe induction of these cytokines in animals that received TPN/si*ID4*. By comparison, mice that received an immunostimulatory siRNA, si*βgal-728* (30), complexed to either lipofectamine or TP-LyP-1 were positive controls for non-specific immunostimulation (fig. S8A). Moreover, we did not observe deleterious effects on animal weight in two ovarian tumor models (fig. S8B), or evidence of macroscopic or histological signs of organ toxicity in the OVCAR-8 orthotopic tumor model (fig. S8C).

DISCUSSION

Current genome characterization efforts will eventually provide insight into the genetic alterations that occur in most cancers, and may define new therapeutic targets. However,

most epithelial cancers harbor hundreds of genetic alterations as a consequence of genomic instability. For example, while recurrent somatic alterations occur in a small number of genes in high-grade ovarian cancers, ovarian cancer genomes are characterized by multiple regions of copy number gain and loss involving at least 1825 genes. This genomic chaos complicates efforts to identify biologically relevant mutations critical for tumor maintenance.

To isolate which recurrent genetic alterations are involved in cancer initiation, tumor maintenance, and/or metastasis, functional assays can be performed following systematic manipulation of the candidate oncogenes. We have combined results from Project Achilles (2), a large scale screening effort to identify genes essential for proliferation and survival in human cancer cell lines with genome characterization of high-grade ovarian cancers. Using this approach, we identified an oncogene candidate, *ID4*, which was amplified in 32% of high-grade serous ovarian cancers. *ID4* is overexpressed in a large fraction of high-grade serous ovarian cancers, and ovarian cancer cell lines that overexpress *ID4* are highly dependent on *ID4* for survival and tumorigenicity. Expression of *ID4* at levels corresponding to those observed in patient-derived samples induced transformation of immortalized ovarian and fallopian tube epithelial cells. Our observations credential *ID4* as an ovarian cancer oncogene and suggest that *ID4* is one of a growing class of lineage-restricted transcriptional factor oncogenes in human epithelial cancers.

Like other ID family proteins, ID4 binds to and regulates the activity of E protein transcription factors such as transcription factors 3 and 12 (TCF3 and TCF12). Indeed, we found that ID4 regulates cell proliferation in part through its effects on $p21^{WAF1/CIP1}$. In addition, the transcriptional program induced by ID4 in ovarian epithelial cells was similar to that induced by HOXA9. Although it is clear that ID4 regulates the expression of many genes, we found that suppression of *HOXA9* abrogated *ID4*-induced cell transformation. HOXA9 is known to regulate normal hematopoiesis by controlling differentiation, proliferation and self-renewal (31), and overexpression of HOXA9 or HOXA9-NUP98 in hematopoietic precursors promotes the development of leukemias (32). In addition, *HOXA* genes have been shown to play essential roles in specifying regional differentiation of mullerian duct into oviduct, uterus, cervix, and vagina (33). Although prior work has shown that manipulation of ID1, ID2 or ID3 expression induces compensatory changes in other ID family members, we found that expression of ID4—but not the other ID family members—induced cell transformation in ovarian epithelial cells. Because amplifications involving other ID family members have not been observed in ovarian cancers, it appears that ID4 plays a unique role in the transformation of this tissue type. Collectively, these findings suggest that inappropriate overexpression of *ID4* may contribute to transformation by affecting both $p21^{WAF1/CIP1}$ and *HOXA9* transcriptional programs that affect differentiation and proliferation programs in the ovary. Nevertheless, further mechanistic studies will be necessary to understand the biology of the new oncogene *ID4* and its downstream target, *HOXA9*.

To credential *ID4* as a therapeutic target in human ovarian cancer, we showed that a tandem peptide with both a membrane-translocating domain (Transportan, TP) and a tumor-penetrating domain (LyP-1) condensed siRNA into nanocomplexes (TPN) that, upon systemic administration into ovarian tumor-bearing mice, penetrated the tumor parenchyma and silenced *ID4* in cells of interest (Fig. 4C). Treatment with TPN/si*ID4* suppressed the growth of ovarian tumors and significantly improved host survival. Previous approaches using inducible shRNAs to evaluate potential cancer targets were time-consuming and required extensive manipulation of cell lines *in vitro* (34-35). Therefore, we favor this modular, tumor-specific, tumor-penetrating approach that delivers siRNA systemically.

Importantly, the TPN are biodegradable and did not elicit innate immune responses upon systemic delivery, enabling repeated administration for tumor regression studies.

Other methods for siRNA delivery include covalent coupling of siRNA to carriers, but this formulation process requires specialized chemically-reactive siRNA and purification steps, obviating the modular 'mix and dose' paradigm motivated by the volume of emerging genomic targets (36). Targeted siRNA delivery has been accomplished in specialized populations such as immune cells, neurons, and hepatocytes; however, these methods are not generalizable across tissue types. Elsewhere, siRNA has been targeted to tumors, but not in a tumor-penetrating fashion (5). For example, tumor endothelium has been targeted using RGD-specific nanoparticles; however, this approach does not enable silencing in parenchymal tumor cells, such as those identified with genetic alterations in TCGA (1). Passive targeting (e.g. EPR effect) of siRNA in neutral liposomes, in complexes with CPP such as TAT, or transferrin-targeted cyclodextrin has also been described in mouse models and recently in humans (37-38), but tumor penetration remained a challenge (39). Our TPN technology represents an important therapeutic paradigm for systemic targeting of "undruggable" proteins that are essential in parenchymal tumor maintenance.

Although we have focused on *ID4*, TPN delivery technology can be generalized to other cancers. Approximately 60 of 81 samples across 10 tumor types exhibit surface expression of p32 (20). Our modular siRNA delivery platform can leverage other homing peptides, such as iRGD, to expand the number and types of TPN-targeted parenchymal tumor cells. More generally, ongoing cancer genome characterization efforts combined with comprehensive functional studies will narrow the number of potential cancer targets, but putative oncogenes will still require validation *in vivo*. TPN offers an efficient platform to verify which genes are critical to cancer initiation and maintenance.

Our studies demonstrate that TPN exhibits both specificity and pharmacokinetic properties that may provide a platform for human siRNA delivery. To reach this goal, additional development is required, such as optimization of circulation time, assessment of efficacy in higher fidelity models of cancer, and reformulation to increase knockdown efficiency and reduce dosing. The path to translating TPN to the clinic will require multi-species toxicity testing, assessment of repeated dosing and potential immunostimulation, and evaluation of the prevalence of the tumor-penetration pathway and p32 in human tumors and metastases.

In summary, we developed a targeted tumor-penetrating nanocomplex capable of precisely delivering siRNA into the tumor parenchyma, and have combined this technology with large-scale methods to credential *ID4* as an oncogene target in ovarian cancer. As large scale efforts to characterize all cancer genomes accelerate, this capability illustrates a path to identify genes that are altered in tumors, validate those that are critical to cancer initiation and maintenance, and rapidly evaluate *in vivo* the subset of such genes amenable to RNAi therapies and clinical translation.

MATERIALS AND METHODS

Pooled shRNA library screen

shRNA constructs are available through Sigma Aldrich. Genome-scale pooled shRNA screens in 102 cancer cell lines were performed using a lentivirally delivered pool of 54,020 shRNAs targeting 11,194 genes. Each cell line was infected in quadruplicate and propagated for at least 16 population doublings (2) (Supplementary Methods). The abundance of shRNAs relative to the initial DNA plasmids was measured by microarray hybridization and normalized using dCHIP and GenePattern modules before identifying essential genes.

Analysis of TCGA data

Copy number alterations were determined by TCGA on 489 primary ovarian tumors using Illumina 1MDUO arrays and recurrently amplified regions were analyzed by GISTIC 2.0 (40) with 99% confidence intervals (Supplementary Methods). For each amplified gene, the distribution of shRNA scores were converted to *z*-score and shRNAs with a $p<0.05$ were identified.

Cell culture

To determine the effects of shRNA on cell proliferation, six replicate infections were performed and viability was determined 5 d later (Supplementary Methods). Transformation was determined by introducing ID4 into immortalized IOSE-M (41) and FTSEC-M cells (16) and performing anchorage-independent growth experiments or monitoring tumor formation by injecting cells subcutaneously into BALB/c immunodeficient mice (Charles River).

Gene expression profiling

Gene expression profiling was performed in triplicate on Affymetrix HG-U133A_2 GeneChips. Processed data from microarray experiments were analyzed using GSEA (42) (Supplementary Methods).

Tumor penetrating nanocomplexes

The tandem peptide library was synthesized *via* standard FMOC solid-phase peptide synthesis and purified by HPLC (Supplementary Methods). Peptides were mixed with siRNA at a molar ratio of 20:1. Nanocomplexes were incubated over cell culture for 4 h and cells were harvested 48h later for characterization of gene knockdown. For competition with free LyP-1, unlabeled LyP-1 peptide was added for 1 h prior to TPN treatment.

Therapeutic studies in mice

TPN carrying *ID4*-specific siRNA were administered intravenously or intraperitoneally to NCr/nude mice bearing either subcutaneous OVCAR-4 or intraperitoneal disseminated OVCAR-8 tumors, respectively. Tumor burdens were monitored *via* caliper measurements or bioluminescence imaging (Supplementary Methods).

Statistical analysis

Unless otherwise indicated, one-way analysis of variance (ANOVA) was used (GraphPad). A P value < 0.05 was considered statistically significant. Fisher's exact test was used for tumor formation assays. Two-tailed Student's t test was used for pair-wise comparisons. A log-rank test was performed for animal survival studies.

Supplementary Material

Refer to Web version on PubMed Central for supplementary material.

Acknowledgments

We thank H. Fleming, A.A. Chen, P. Sharp, and E. Lander for critical readings of the manuscript (MIT). We thank D. Livingston for the luciferized OVCAR-8 cells and valuable insight into ovarian cancer (DFCI). **Funding:** Supported by the Howard Hughes Medical Institute (S.N.B.), National Cancer Institute U54 CA119349 (S.N.B.), U54 CA119335 (S.N.B.), R01 CA124427 (S.N.B), R33 CA128625 (W.C.H.), RC2 CA148268 (W.C.H.), U54 CA112962 (W.C.H.), RO1 CA152327 (E.R.), P50 CA105009 (R.D.), NIH U01 CA152990 (R.D.), Starr Cancer Consortium (W.C.H. And S.N.B.), The Marie-D. & Pierre Casimir-Lambert Fund (S.N.B), The Mary Kay

Foundation (R.D.), the Sandy Rollman Ovarian Cancer Foundation (R.D.), Canadian Institutes of Health Research Fellowship (A.M.K.), and partially by Cancer Center Support (core) Grant P30 CA14051 from the NCI.

REFERENCES AND NOTES

1. The Cancer Genome Atlas Research Network. Integrated genomic analyses of ovarian carcinoma. Nature. Jun 30.2011 474:609. [PubMed: 21720365]
2. Cheung HW, et al. Systematic investigation of genetic vulnerabilities across cancer cell lines reveals lineage-specific dependencies in ovarian cancer. Proc Natl Acad Sci U S A. Jul 26.2011 108:12372. [PubMed: 21746896]
3. Elbashir SM, et al. Duplexes of 21-nucleotide RNAs mediate RNA interference in cultured mammalian cells. Nature. May 24.2001 411:494. [PubMed: 11373684]
4. Fire A, et al. Potent and specific genetic interference by double-stranded RNA in Caenorhabditis elegans. Nature. Feb 19.1998 391:806. [PubMed: 9486653]
5. Whitehead KA, Langer R, Anderson DG. Knocking down barriers: advances in siRNA delivery. Nat Rev Drug Discov. Feb.2009 8:129. [PubMed: 19180106]
6. Hambley TW, Hait WN. Is anticancer drug development heading in the right direction? Cancer Res. Feb 15.2009 69:1259. [PubMed: 19208831]
7. Minchinton AI, Tannock IF. Drug penetration in solid tumours. Nat Rev Cancer. Aug.2006 6:583. [PubMed: 16862189]
8. Olive KP, et al. Inhibition of Hedgehog signaling enhances delivery of chemotherapy in a mouse model of pancreatic cancer. Science. Jun 12.2009 324:1457. [PubMed: 19460966]
9. Provenzano PP, et al. Enzymatic targeting of the stroma ablates physical barriers to treatment of pancreatic ductal adenocarcinoma. Cancer Cell. Mar 20.2012 21:418. [PubMed: 22439937]
10. Teesalu T, Sugahara KN, Kotamraju VR, Ruoslahti E. C-end rule peptides mediate neuropilin-1-dependent cell, vascular, and tissue penetration. Proc Natl Acad Sci U S A. Sep 22.2009 106:16157. [PubMed: 19805273]
11. Roth L, et al. Transtumoral targeting enabled by a novel neuropilin-binding peptide. Oncogene. Dec.19:2011.
12. van den Berg A, Dowdy SF. Protein transduction domain delivery of therapeutic macromolecules. Curr Opin Biotechnol. Apr.11:2011.
13. Sugahara KN, et al. Coadministration of a tumor-penetrating peptide enhances the efficacy of cancer drugs. Science. May 21.2010 328:1031. [PubMed: 20378772]
14. Boehm JS, et al. Integrative genomic approaches identify IKBKE as a breast cancer oncogene. Cell. Jun 15.2007 129:1065. [PubMed: 17574021]
15. Levanon K, Crum C, Drapkin R. New insights into the pathogenesis of serous ovarian cancer and its clinical impact. J Clin Oncol. Nov 10.2008 26:5284. [PubMed: 18854563]
16. Karst AM, Levanon K, Drapkin R. Modeling high-grade serous ovarian carcinogenesis from the fallopian tube. Proc Natl Acad Sci U S A. May 3.2011 108:7547. [PubMed: 21502498]
17. Takeda A, Goolsby C, Yaseen NR. NUP98-HOXA9 induces long-term proliferation and blocks differentiation of primary human CD34+ hematopoietic cells. Cancer Res. Jul 1.2006 66:6628. [PubMed: 16818636]
18. Faber J, et al. HOXA9 is required for survival in human MLL-rearranged acute leukemias. Blood. Mar 12.2009 113:2375. [PubMed: 19056693]
19. Wu Q, et al. Transcriptional regulation during p21WAF1/CIP1-induced apoptosis in human ovarian cancer cells. J Biol Chem. Sep 27.2002 277:36329. [PubMed: 12138103]
20. Fogal V, Zhang L, Krajewski S, Ruoslahti E. Mitochondrial/cell-surface protein p32/gC1qR as a molecular target in tumor cells and tumor stroma. Cancer Res. Sep 1.2008 68:7210. [PubMed: 18757437]
21. Laakkonen P, et al. Antitumor activity of a homing peptide that targets tumor lymphatics and tumor cells. Proc Natl Acad Sci U S A. Jun 22.2004 101:9381. [PubMed: 15197262]
22. Maurer-Stroh S, Eisenhaber F. Myristoylation of viral and bacterial proteins. Trends Microbiol. Apr.2004 12:178. [PubMed: 15051068]

23. Agrawal A, et al. Functional delivery of siRNA in mice using dendriworms. ACS Nano. Sep 22.2009 3:2495. [PubMed: 19673534]
24. Lindberg M, Jarvet J, Langel U, Graslund A. Secondary structure and position of the cell-penetrating peptide transportan in SDS micelles as determined by NMR. Biochemistry. Mar 13.2001 40:3141. [PubMed: 11258929]
25. Moghimi SM, Hunter AC, Murray JC. Long-circulating and target-specific nanoparticles: theory to practice. Pharmacol Rev. Jun.2001 53:283. [PubMed: 11356986]
26. Koivunen E, Wang B, Ruoslahti E. Phage libraries displaying cyclic peptides with different ring sizes: ligand specificities of the RGD-directed integrins. Biotechnology (NY). Mar.1995 13:265.
27. von Maltzahn G, et al. In vivo tumor cell targeting with “click” nanoparticles. Bioconjug Chem. Aug.2008 19:1570. [PubMed: 18611045]
28. Prabhu S, Ignatova A, Park ST, Sun XH. Regulation of the expression of cyclin-dependent kinase inhibitor p21 by E2A and Id proteins. Mol. Cell Biol. Oct.1997 17:5888. [PubMed: 9315646]
29. Huang YH, et al. Claudin-3 gene silencing with siRNA suppresses ovarian tumor growth and metastasis. Proc Natl Acad Sci U S A. Mar 3.2009 106:3426. [PubMed: 19208807]
30. Judge AD, et al. Sequence-dependent stimulation of the mammalian innate immune response by synthetic siRNA. Nat Biotechnol. Apr.2005 23:457. [PubMed: 15778705]
31. Abramovich C, Humphries RK. Hox regulation of normal and leukemic hematopoietic stem cells. Curr Opin Hematol. May.2005 12:210. [PubMed: 15867577]
32. Ono R, et al. Mixed-lineage-leukemia (MLL) fusion protein collaborates with Ras to induce acute leukemia through aberrant Hox expression and Raf activation. Leukemia. Dec.2009 23:2197. [PubMed: 19710696]
33. Kobayashi A, Behringer RR. Developmental genetics of the female reproductive tract in mammals. Nat Rev Genet. Dec.2003 4:969. [PubMed: 14631357]
34. Cheung HW, et al. Amplification of CRKL Induces Transformation and Epidermal Growth Factor Receptor Inhibitor Resistance in Human Non-Small Cell Lung Cancers. Cancer Discov. Dec.2011 1:608. [PubMed: 22586683]
35. Kappel S, Matthess Y, Kaufmann M, Strebhardt K. Silencing of mammalian genes by tetracycline-inducible shRNA expression. Nat Protoc. 2007; 2:3257. [PubMed: 18079726]
36. Henke E, et al. Peptide-conjugated antisense oligonucleotides for targeted inhibition of a transcriptional regulator in vivo. Nat Biotechnol. Jan.2008 26:91. [PubMed: 18176556]
37. Davis ME, et al. Evidence of RNAi in humans from systemically administered siRNA via targeted nanoparticles. Nature. Apr 15.2010 464:1067. [PubMed: 20305636]
38. Medarova Z, Pham W, Farrar C, Petkova V, Moore A. In vivo imaging of siRNA delivery and silencing in tumors. Nature medicine. Mar.2007 13:372.
39. Ruoslahti E, Bhatia SN, Sailor MJ. Targeting of drugs and nanoparticles to tumors. J Cell Biol. Mar 22.2010 188:759. [PubMed: 20231381]
40. Mermel CH, et al. GISTIC2.0 facilitates sensitive and confident localization of the targets of focal somatic copy-number alteration in human cancers. Genome Biol. Apr 28.2011 12:R41. [PubMed: 21527027]
41. Liu J, et al. A genetically defined model for human ovarian cancer. Cancer Res. Mar 1.2004 64:1655. [PubMed: 14996724]
42. Subramanian A, et al. Gene set enrichment analysis: a knowledge-based approach for interpreting genome-wide expression profiles. Proc. Natl Acad. Sci. USA. Oct 25.2005 102:15545. [PubMed: 16199517]

ONE SENTENCE SUMMARY

Tumor-penetrating siRNA nanocomplexes credentials *ID4* as a therapeutic oncogene target in human ovarian cancer.

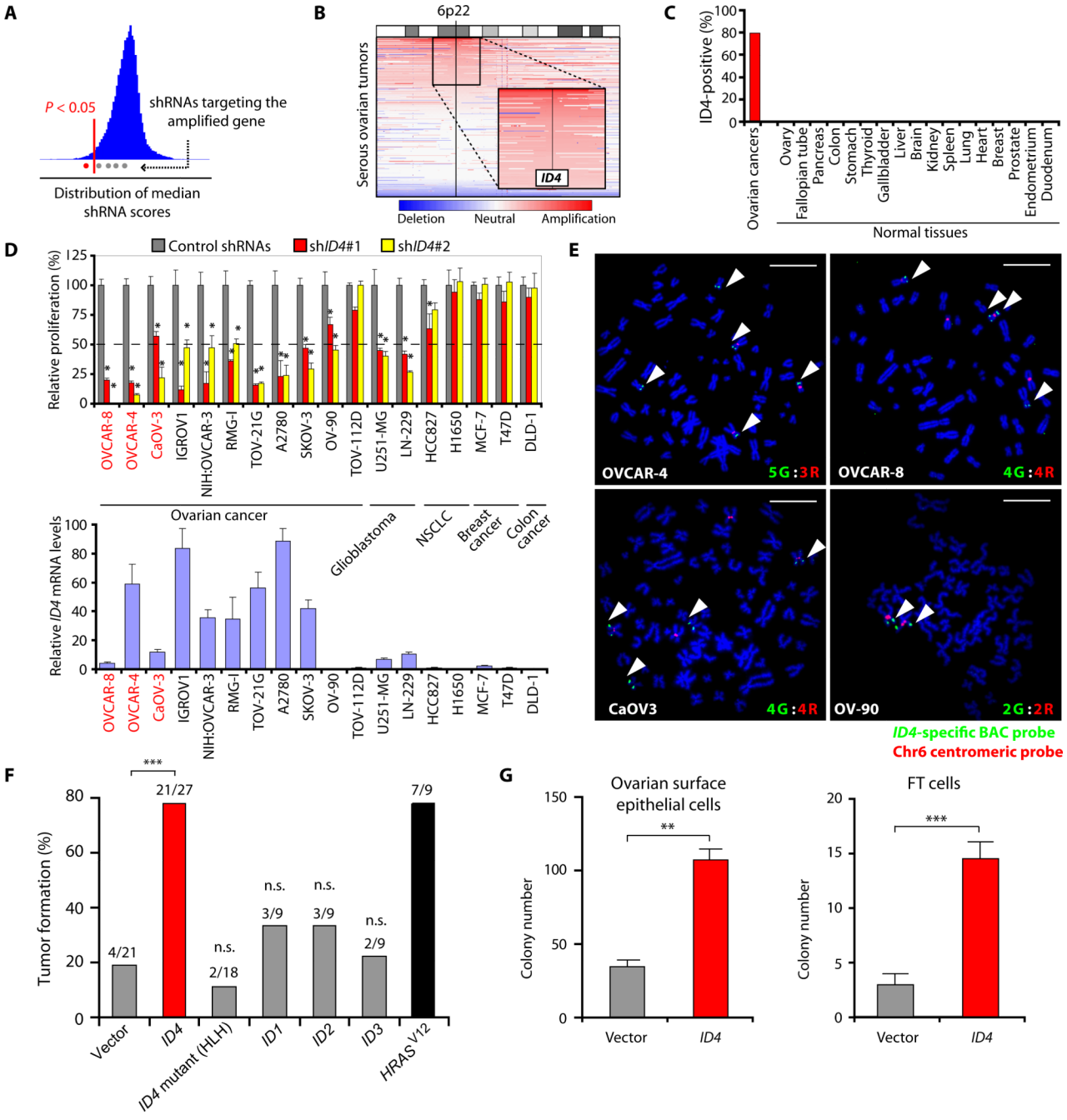

Figure 1. *ID4* is essential for the proliferation of ovarian cancer cells

(**A**) Median shRNA depletion scores for each amplified gene. Schematic shows the distribution of median shRNA scores (blue bars) in cell lines that harbor copy number gain ($\log_2$ copy number ratio > 0.3) of a given gene. shRNAs targeting the amplified gene (dots) are considered significant if p <0.05 (red line). This analysis was repeated for each of 1825 amplified genes in 63 recurrent regions of genomic amplification identified in primary ovarian tumors. (**B**) Amplification of *ID4* in primary high-grade serous ovarian tumors. SNP array colorgram depicts genomic amplification of *ID4* at chromosome 6p22 region in subsets of primary ovarian tumors, sorted on the basis of the degree of amplification. (**C**) Immunohistochemical analysis of ID4 performed on sections from tissue microarrays

composed of primary human ovarian cancers (n=131) and normal tissues (n=85). (**D**) Effects of *ID4* suppression by two different shRNAs on proliferation of human cancer cell lines (top) and relative levels of *ID4* mRNA (bottom). Data are averages ± s.d. (n = 6 replicate measurements). 6p22-amplified lines are marked in red. *p<0.05 compared to shGFP (control), Student's t test. (**E**) FISH analysis of ID4 in ovarian cancer cells. (**F**) Potentiation of tumorigenicity by *ID4* overexpression. IOSE-M cells expressing the indicated constructs were implanted subcutaneously into immunodeficient mice. The number of tumors formed/injections is indicated. $HRAS^{V12}$-expressing IOSE cells were used as a positive control. ***p<0.001, n.s., not significant, Fisher's exact test. (**G**) *ID4* promotes anchorage-independent growth of IOSE-M (ovarian epithelial) and FTSEC-M (fallopian tube) cells. Data are averages ± s.d. (n = 6). **p<0.01, ***p<0.001 compared to respective vector control, Student's t test.

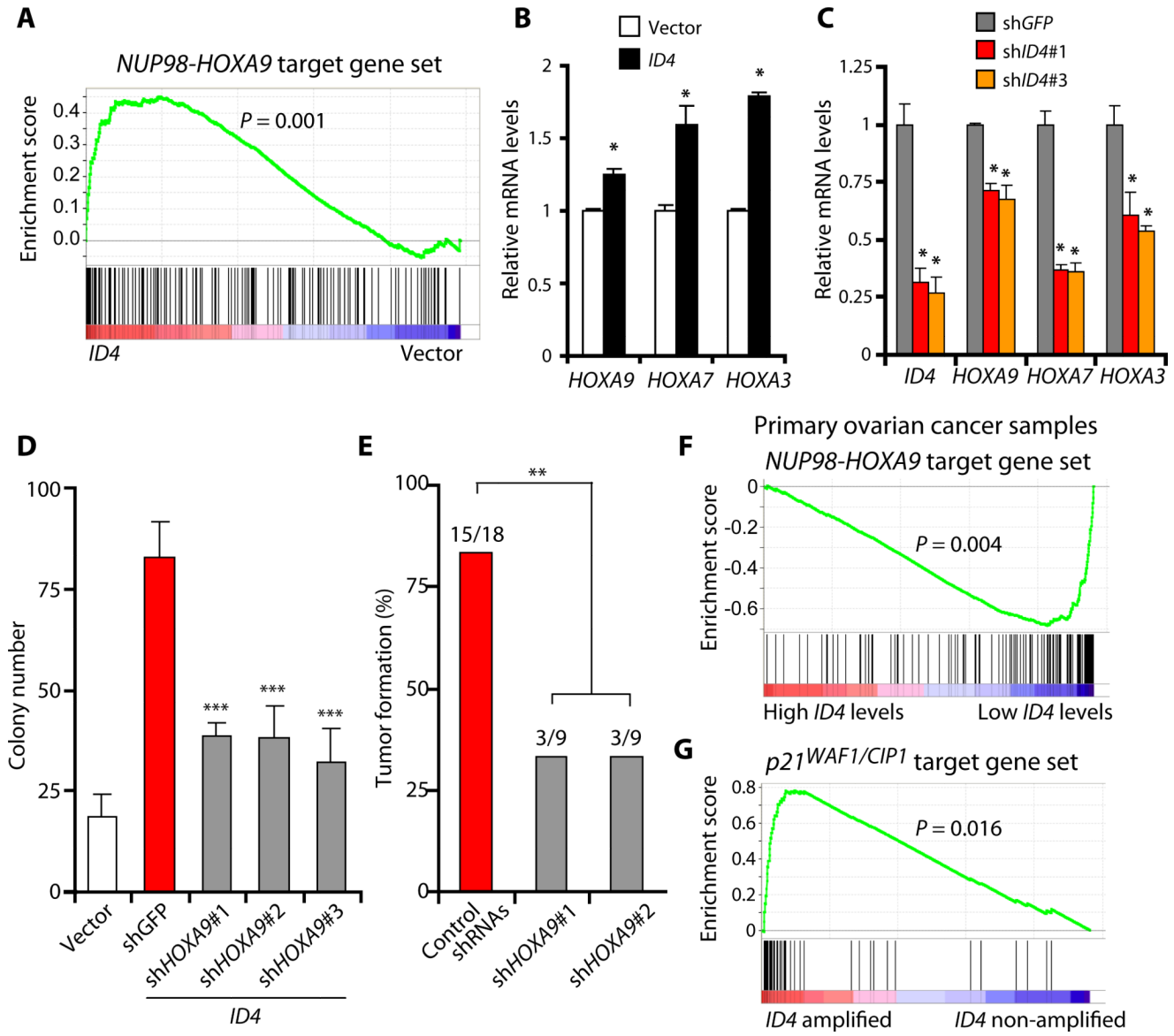

Figure 2. *ID4* induces tumorigenicity that depends on *HOXA9*

(**A**) *ID4* induces *HOXA9* gene activity. Gene expression profiling and gene set enrichment analysis (GSEA) were performed on IOSE-M cells overexpressing *ID4* or a control vector. All genes were ranked on the basis of the differential expression between cells expressing *ID4* or a control vector. Black bars at the bottom of the figure indicate the location of genes in a *NUP98-HOXA9* upregulated gene set (TAKEDA_TARGETS_of_NUP98_HOXA9_FUSION_3D_UP) (17) within the ranked list and the green curve indicates the running enrichment score for the gene set. (**B**) Quantitative RT-PCR analysis of *HOXA9, HOXA7*, and *HOXA3* mRNA in IOSE-M cells overexpressing *ID4* or a control empty vector. Data are averages ± s.d. ($n = 6$ replicate measurements). (**C**) Quantitative RT-PCR analysis of *HOXA9, HOXA7*, and *HOXA3* mRNA in OVCAR-8 cells 3 days after infection with a control sh*GFP* or two shRNAs targeting *ID4*. Data are averages ± s.d. ($n = 6$ replicate measurements). (**D**) Anchorage-independent growth of *ID4*-overexpressing IOSE-M cells in response to sh*HOXA9*. Data are averages ± s.d. ($n = 6$). ***$p<0.0001$, Student's *t* test. (**E**) The effect of *HOXA9*

suppression on *ID4*-induced tumorigenicity in immunodeficient mice. *ID4*-overexpressing IOSE-M cells expressing indicated shRNAs were subcutaneously implanted into immunodeficient mice. The number of tumors formed/injections is indicated. $^{**}p<0.01$, Fisher's exact test. (**F**) Expression data from primary ovarian tumors with low *ID4* expression levels ($n = 44$ samples) were compared to samples with high *ID4* expression ($n = 45$). Thresholds were 1 s.d. below and above the mean expression of all the samples. At the bottom of the enrichment plots, black bars indicate the location of genes in a *NUP98-HOXA9*-downregulated gene set (TAKEDA_TARGETS_OF_NUP98_HOXA9_FUSION_10D_DN) (17). (**G**) *ID4* amplification in ovarian tumors correlated with decreased $p21^{WAF1/CIP1}$ activity. Expression profiling of primary ovarian tumors with matched copy number data was used to perform GSEA on amplified *ID4* ($\log_2$ copy number ratio >0.3) and non-amplified *ID4* samples ($\log_2$ copy number ratio <0). All genes were ranked by their differential expression (signal to noise) between 81 non-amplified and 109 amplified *ID4* primary tumors. Black bars at the bottom of the figure indicate the location of genes in the $p21^{WAF1/CIP1}$ target gene set (P21_P53_ANY_DN).

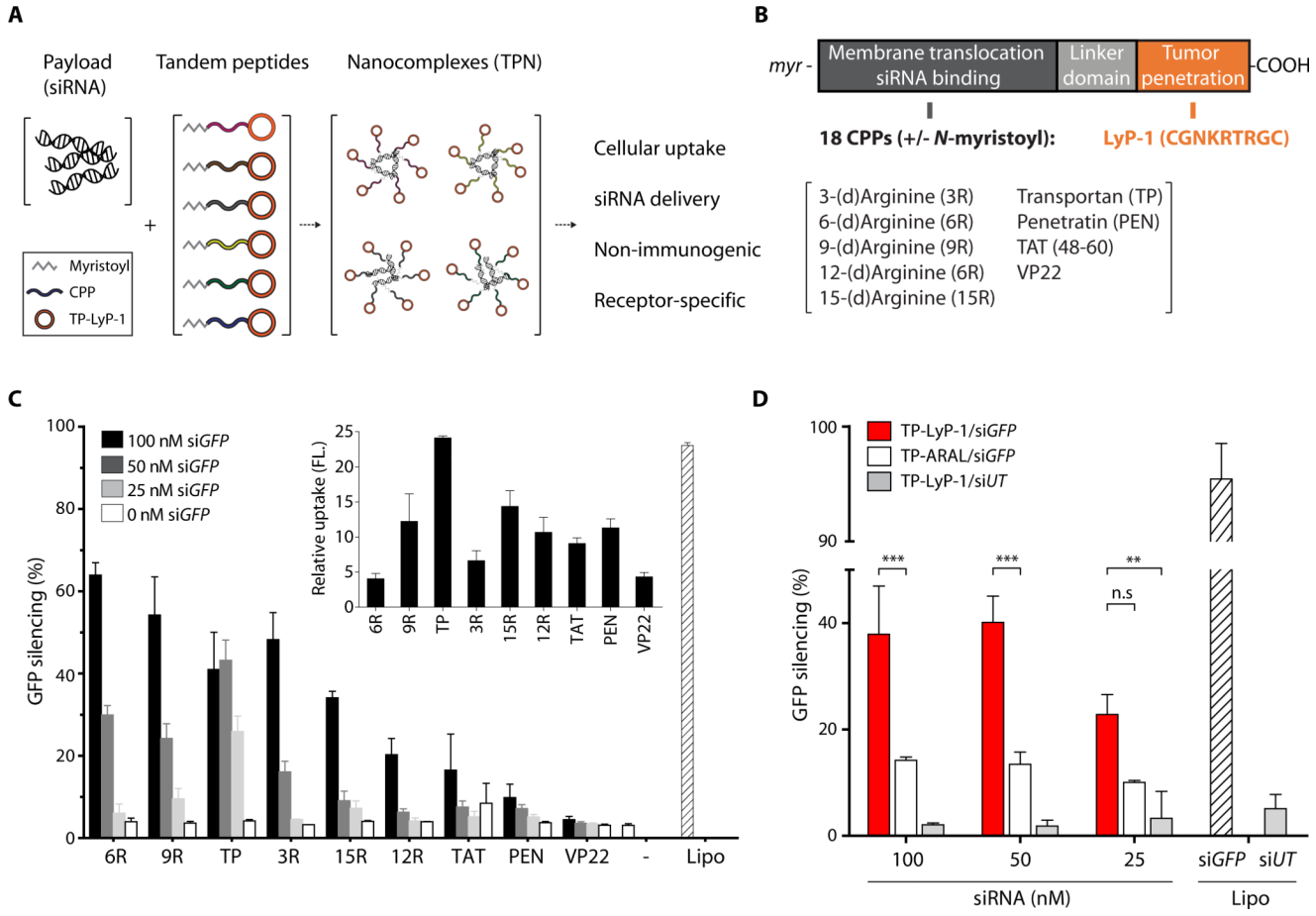

Figure 3. Characterization and activity of tumor-penetrating nanocomplexes (TPN)

(**A**) Schematic of the tandem peptide screen. siRNA was noncovalently bound to a library of 18 candidate tandem peptides bearing a fixed *N*-terminal cyclic tumor-penetration domain and variable *C*-terminal linear membrane translocation domains. The resulting nanocomplexes were assayed and selected for their cellular uptake, siRNA delivery, lack of immunogenicity, and receptor specificity in human cancer cell lines *in vitro* or in mouse models of human ovarian cancer. (**B**) The tandem peptide construct and various membrane translocation domains tested. (**C**) Gene silencing activity of tandem peptide-si*GFP* nanocomplexes in HeLa cells stably expressing GFP. Percent GFP silencing was calculated based on the geometric mean of GFP fluorescence intensity of the whole population relative to cells treated with media only. The lipofectamine control (Lipo) contained 100 nM GFP-siRNA. Data are averages ± s.d ($n = 4$ independent experiments). Inset: HeLa cell uptake of fluorescently labeled nanocomplexes was assessed by flow cytometry. Data are averages ± s.d ($n = 4$ independent experiments). (**D**) Receptor specificity of nanocomplex-mediated GFP silencing. Data are averages ± s.d ($n = 6$ independent experiments). $^{**}p<0.01$; $^{***}p<0.001$, n.s., not significant, one-way ANOVA.

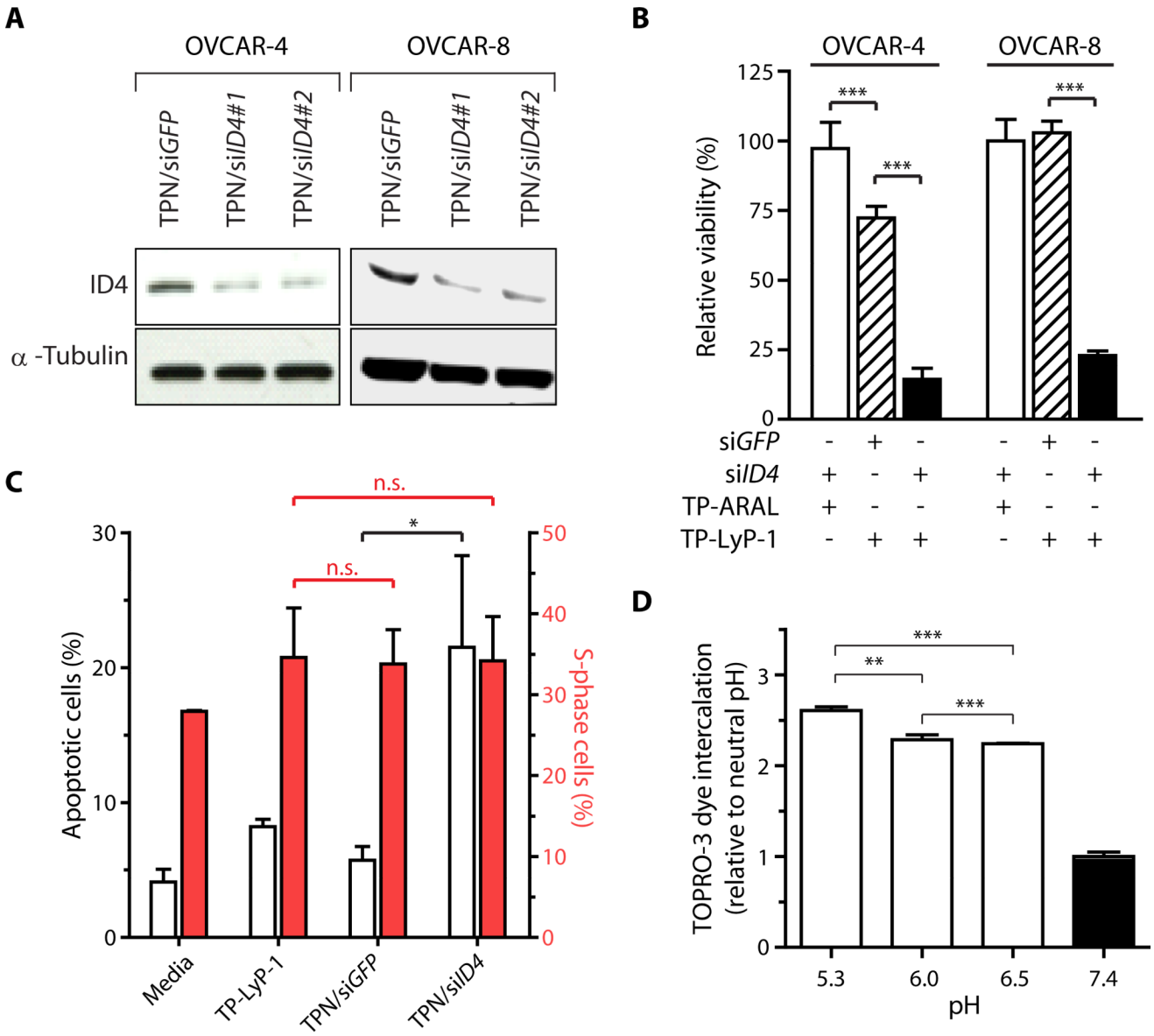

Figure 4. TPN mediated suppression of ID4 in p32-expressing ovarian cancer cells

(A) *ID4* suppression by TPN-mediated siRNA delivery *in vitro*. Immunoblot of ID4 in two 6p22-amplified ovarian cancer cell lines, OVCAR-4 and OVCAR-8, which were treated with TPN containing one of two *ID4*-specific siRNAs or a control siRNA targeting GFP (si*GFP*). α-Tubulin was used as a loading control. **(B)** Effects of *ID4* suppression on cell proliferation. Data are averages ± s.d. ($n = 4$ independent experiments). ***$p<0.001$, one-way ANOVA. (**C**) Effects of *ID4* suppression in OVCAR-8 cells. The percentages of apoptotic and S-phase cells were calculated. Data are averages ± s.d. ($n = 3$ independent experiments). *$p<0.05$, n.s., not significant. one-way ANOVA. **(D)** Intercalation of TO-PRO-3, a nucleic acid-binding dye, into siRNA in the presence of TPN at various pH. Fluorescence was detected at 640/680 nm (ex/em). Data are averages ± s.d. ($n = 4$ independent experiments). **$p<0.01$, ***$p<0.001$, one-way ANOVA and Tukey post-hoc tests.

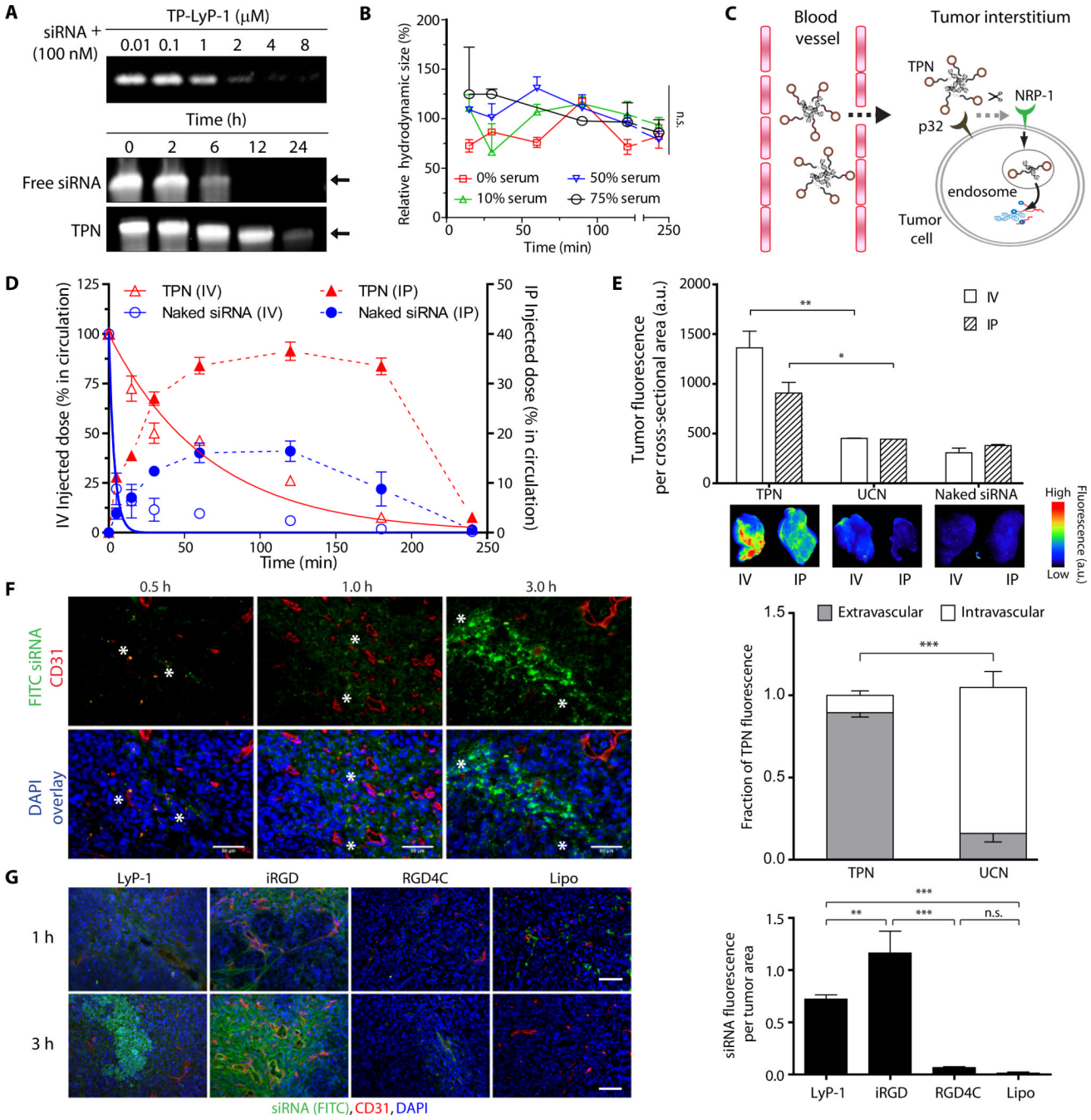

Figure 5. TPN homing *in vivo*

(**A**) Serum stability of TPN. (Top) Agarose gel analysis of siRNA complexed to TP-LyP-1 at varying molar ratios. (Bottom) Gel electrophoresis of free siRNA and TPN in mouse serum at 37°C at the indicated times. Arrow indicates expected position of intact siRNA (14 kDa). (**B**) Dynamic light scattering measurements of TPN in varying concentrations of mouse serum at 37°C over time. The hydrodynamic diameter of TPN in each serum concentration over time is normalized to its size in PBS (0% serum) at time 0 min. Data are averages ± s.d. (n = 6 independent measurements). n.s., not significant, one-way ANOVA. **(C)** Schematic of TPN penetration and targeted delivery of siRNA into the cytosol of cancer cells. (**D**) *In vivo* circulation of TPN compared with naked siRNA against GFP upon

intravenous (IV) or intraperitoneal (IP) administration. Fluorescence of siRNA was detected in the blood drawn retro-orbitally. Data are averages ± s.d. ($n = 3$). (**E**) Quantification of siRNA fluorescence and corresponding fluorescence images of MDA-MB-435 whole-tumor explants harvested 4 h after injection of TPN, UCN, or naked siRNA, either IV or IP. Data are averages ± s.d. (n=6). *$p<0.05$; **$p<0.01$, one-way ANOVA. (**F**) Histological analysis of time-dependent homing of TPN carrying FITC-labeled siRNA (asterisks) in relation to blood vessels in mice bearing human OVCAR-8 tumor xenografts. Nuclei were stained with DAPI. Tumor vasculature is CD31+. Scale bars, 50 μm. On the right, extravascular and intravascular fractions of TPN were quantified from the fluorescence images. Data are averages ± s.d., from representative sections of 6 independent tumors. ***$p<0.001$ by two-tailed Student's *t*-test. (**G**) Tumor parenchyma penetration by TPN with LyP-1 and iRGD homing domains, non-penetrating nanocomplex targeted by RGD4C peptide, and lipofectamine. Nanocomplexes were injected intravenously and OVCAR-8 tumors were stained 1 or 3 h later (n = 6 per formulation). Scale bars, 50 μm. On the right, tumor fluorescence was quantified. Data are averages ± s.d. from 6 randomly selected views per condition. **$p<0.01$; ***$p<0.001$, n.s., not significant, by one-way ANOVA with Tukey post-hoc tests.

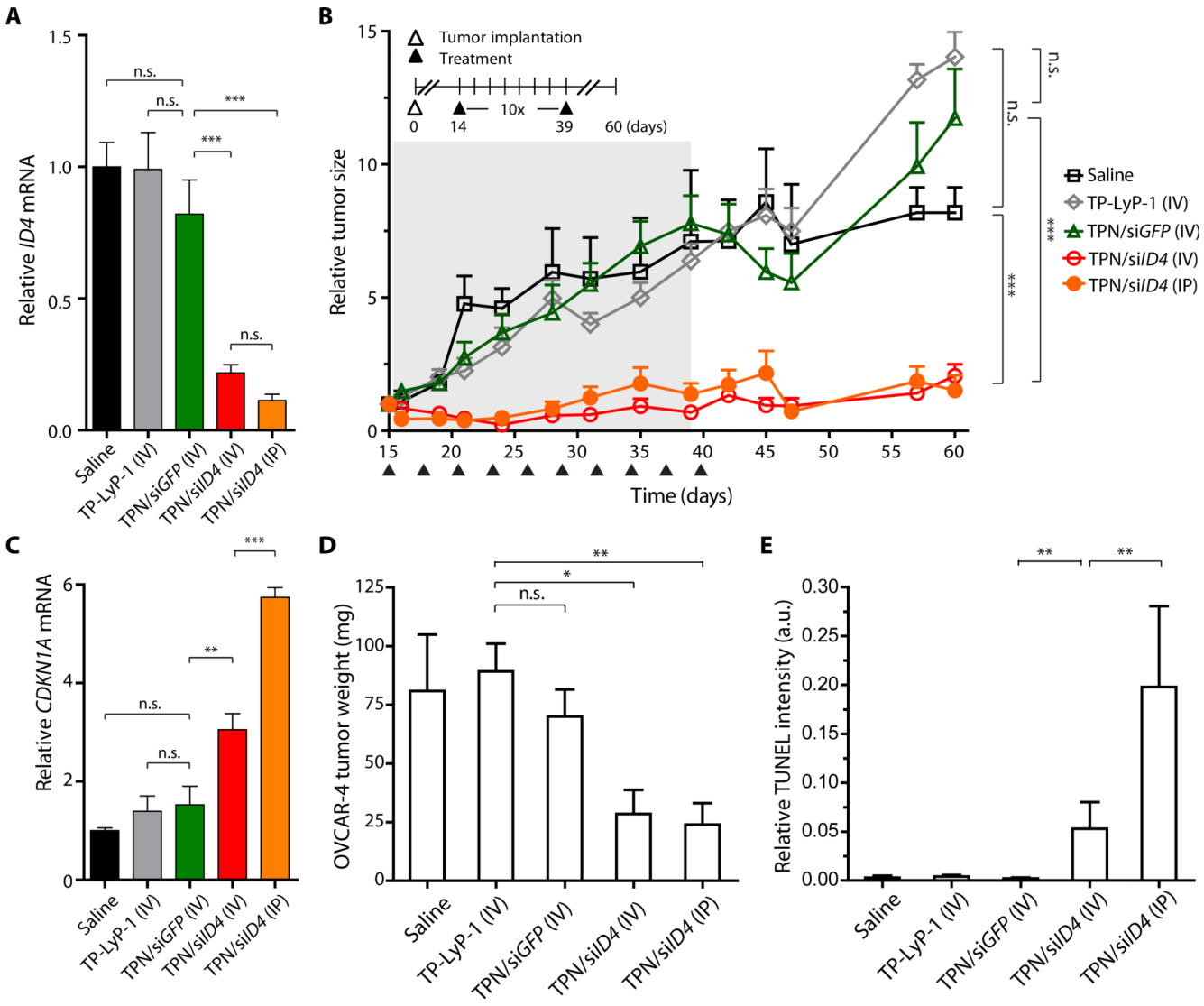

Figure 6. Subcutaneous tumor treatment with TPN/si*ID4*

(**A, B**) Efficacy of TPN-mediated delivery of si*ID4 in vivo*. *ID4* mRNA (A) and burden of subcutaneous OVCAR-4 xenografts (B) after treatments with the indicated formulations every 3 days for 25 days (arrowheads). Control cohorts received either TP-LyP-1 without siRNA or TPN/si*GFP*. Inset shows the experimental timeline. Treatment period is shaded in gray. Data are averages ± s.d. (n = 8-10 tumors per group). ***p<0.001, n.s., not significant, one-way ANOVA. (**C**) *CDKN1A* mRNA levels from tumors at day 60, relative to saline control. Data are averages ± s.d. **p<0.01; ***p<0.001, n.s., not significant, one-way ANOVA. (**D**) Weight of OVCAR-4 tumors at day 60. Data are averages ± s.d. (n = 5-10 tumors per cohort). *p<0.05, **p<0.01, n.s., not significant, one-way ANOVA. (**E**) Quantification of TUNEL staining intensities from 6-10 randomly selected OVCAR-4 tumor sections (n = 5 per treatment group) after 30 days of TPN treatment. Data are averages ± s.d. **p<0.01, one-way ANOVA

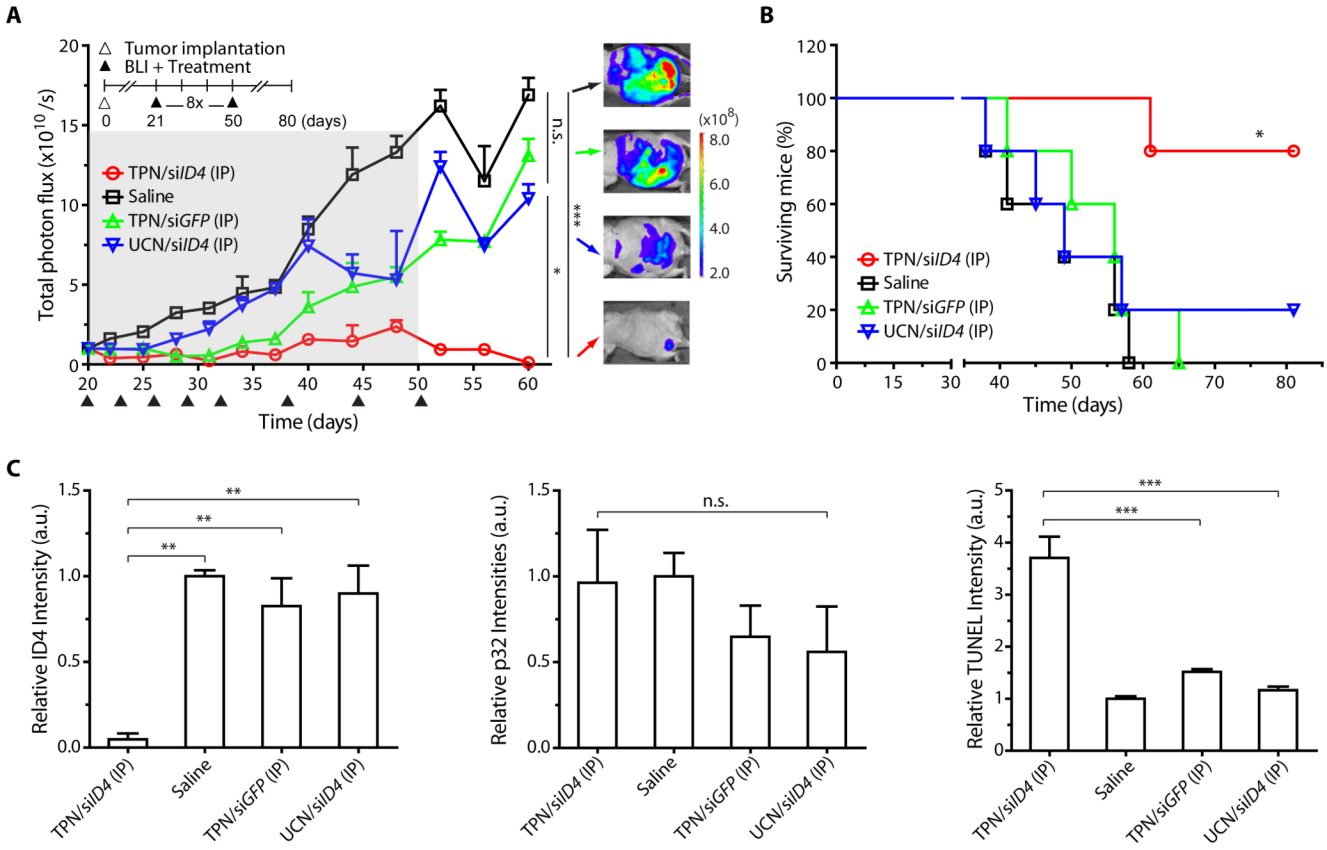

Figure 7. Orthotopic tumor treatment with TPN/si*ID4*

(**A**) Therapeutic efficacy of TPN in mice bearing disseminated orthotopic OVCAR-8 tumors. Mice were treated i.p. every 3 days for 14 days and then once weekly thereafter for 3 weeks with TPN/si*ID4*, saline, TPN/si*GFP*, and UCN/si*ID4* (arrowheads). Inset shows the experimental timeline. Total tumor burden was followed by bioluminescence imaging, with images from day 60 shown. Data are means ± s.d. (n = 5 mice per group). *p<0.05; ***p<0.001, n.s., not significant, one way ANOVA. (**B**) Kaplan-Meier plot of overall survival of the cohorts shown in (D). *p<0.05 by Log-rank (Mantel-Cox) Test. (**C**) Quantification of ID4, p32, and TUNEL intensities from OVCAR-8 tumors on day 4. Intensity values are normalized to that of saline controls. Data are averages ± s.d. (n = 5 per treatment group). **p<0.01, ***p<0.001, n.s., not significant, one-way ANOVA.